Computer Assisted Mechanics and Engineering Sciences, 14: 67–78, 2007.

Modelling of crystal plasticity effects on the crack initiation energies of a bi-crystal interface (Nb/Al_2O_3)

Amir Siddiq, Siegfried Schmauder
Institut für Materialprüfung, Werkstoffkunde und Festigkeitslehre (IMWF)
University of Stuttgart, Germany

(Received March 31, 2005)

The present paper examines the crystal orientation effects on the energy at the crack-tip of niobium/alumina joints. The analyses have been done using crystal plasticity theory. The single crystal parameters are identified for each family of slips system in [21]. These identified parameters are being used to examine the orientation effects of the niobium single crystal on the energy at the crack-tip. Differences in the fracture energy are explained based on the plastic slip (strain) induced in different slip systems during deformation. A qualitative comparison of the crystal plasticity analysis with the experiments of [4, 15] is also been presented.

Keywords: crystal plasticity, finite element methods, fracture, metal–ceramic interface

1. INTRODUCTION

Metal/ceramic bimaterials with a mismatch in mechanical properties are frequently encountered in engineering applications. In many of these situations cracks initiate at interfaces and advance along or away from the interfaces. The safety of such components inevitably requires a thorough understanding of their behaviour under load.

The J-integral method is widely used in rate-independent quasi-static fracture analyses to characterize the energy release rate associated with crack growth [3, 6]. The J-integral method was introduced by Rice [20] in 1968, since then J-based elastic plastic fracture mechanics became also an issue of numerical computations [9, 10, 16, 17, 23]. In the beginning the user were left to their own codes, which gave rise to additional uncertainties and errors. Brock and Scheider [3] explained the procedure to obtain reliable values of J-integral when used in ABAQUS [1].

The J-integral is widely accepted as a fracture mechanics parameter for both linear and nonlinear material response. Cherepanov [5] and Rice [20] were the first two who introduced path-independent integrals into fracture mechanics [3]. Rice also showed that this "J-integral" is identical with the energy release rate

$$J = G = -\left(\frac{\partial U}{\partial a}\right) \tag{1}$$

for a plane crack extension, Δa.

The J-integral is defined in terms of the energy release rate, associated with a fictitious small crack advance, Δa, Fig. 1,

$$J = \frac{1}{\Delta a_c} \iint_{\beta_0} [\sigma_{ij} u_{j,k} - W \delta_{ik}] \, \Delta x_{k,i} \, \mathrm{d}S, \tag{2}$$

where Δx_k is the shift of the crack front coordinates from the initial crack tip, Δa_c the correspondent increase in crack area and the integration domain β_0 is the grey area in Fig. 1.

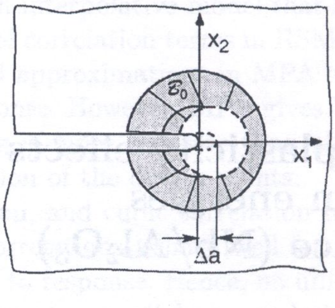

Fig. 1. Domain for J-Integral

2. EXPERIMENTAL PROCEDURE

The finite element model is based on the experiments performed in [4, 15], in which the influence of orientation and impurities on the fracture behaviour of Nb-sapphire interfaces were studied using notched bending tests. Single crystals were diffusion bonded in ultra high vacuum furnace for different interface orientations. For undoped bicrystals bonded at 1400°C, the computed interfacial fracture energy ranged from 77 to 2100 $\mathrm{J/m^2}$ depending on the interface planes of Nb and sapphire. For fracture evaluation, interfacially notched bending test specimens of dimensions $2{\times}4{\times}32\,\mathrm{mm}^3$ were prepared. The specimen is shown in Fig. 2. The notch length is 0.4 mm. The specimen is loaded to the fracture load F_c in a four-point bending tests device at a cross-head speed of 96.8 μm/min. The load F and the cross-head deflection at the load points v are simultaneously recorded.

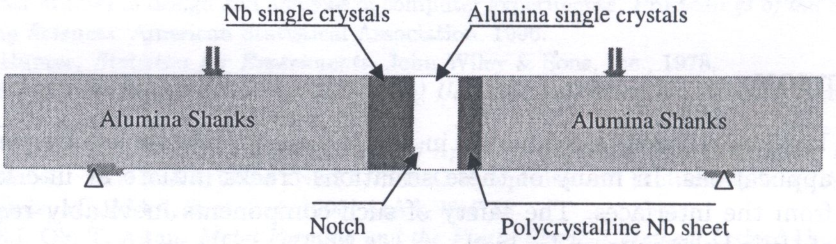

Fig. 2. Four point bending test specimen

3. FINITE ELEMENT ANALYSIS

Finite element simulations were done using three-dimensional model, the finite element mesh consisted of twenty-noded quadratic reduced integration elements. The total number of elements in the model is 17208. The mesh is shown in Fig. 3.

For all three-dimensional simulations, both outer Alumina shanks (ceramic) and Alumina single crystal at the middle of the specimen were treated as purely elastic with a Young's modulus of 390 GPa and a Poisson's ratio of 0.27. The polycrystalline niobium sheet is always modelled with an elastic-plastic constitutive law. The Young's modulus and the Poison's ratio were the same for all simulations ($E = 104.9\,\mathrm{GPa}$, $\nu = 0.397$). These elastic data are adjusted to alumina and niobium, respectively [11–13]. The plastic behaviour of the stress-strain curve of the polycrystalline niobium sheet is approximated by a Ramberg–Osgood relation [19], which is described in the one-dimensional case by the following equation,

$$E_c = \sigma + \alpha \left(\frac{\sigma}{\sigma_0} \right)^{n-1} \sigma \, . \tag{3}$$

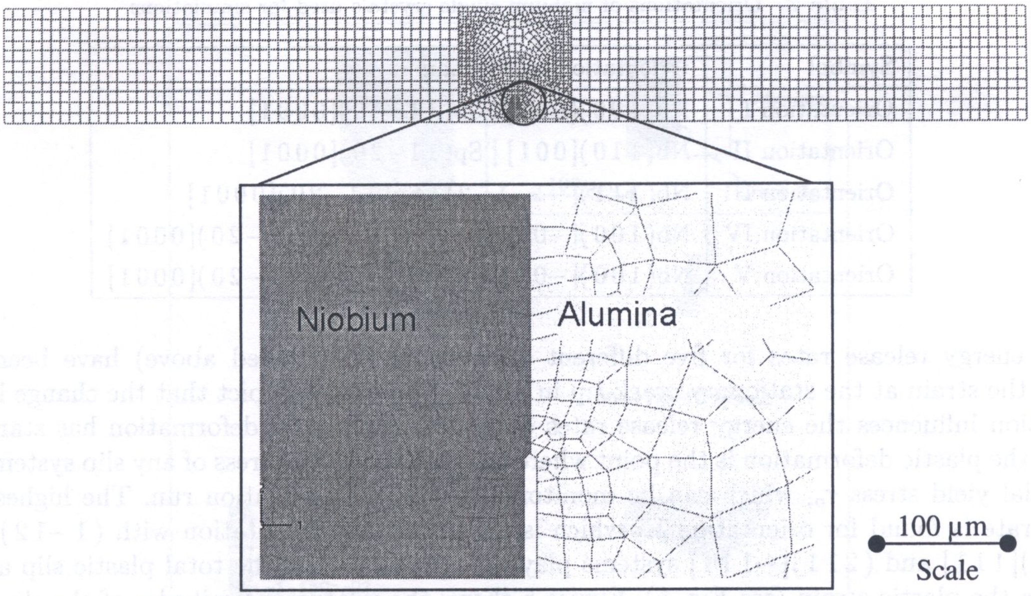

Fig. 3. Three dimensional finite element mesh of bimaterial specimen

Here, n denotes the hardening exponent, α the yield offset and σ_0 the yield stress. This material law is nonlinear from the beginning, but for commonly used hardening exponents ($n \geq 5$) the divergence from linearity is only slight for stresses below σ_0. The chosen plasticity theory is the deformation plasticity theory (for details see [18] and references therein), which describes not a plastic material behaviour, but a nonlinear elastic material. This means, that no unloading criterion exists. The parameters of the above equation are adjusted to the niobium stress-strain curves in [14]. The parameters used are $n = 6$, $\sigma_0 = 180\,\mathrm{MPa}$ and $\alpha = 0.3$.

For the case of crystal plasticity [7, 8], the single crystal niobium is modelled using the hardening law of Bassani & Wu [2, 24]. The hardening parameters for each slip system are derived in [21] and are given in Table 1

A four point bending test has been simulated with the boundary conditions as shown in Fig. 3. The displacement of 30 μm is applied stepwise (increasing linearly with time) at the loading points.

Table 1. Hardening parameters for Bassani & Wu hardening law

	τ_o (MPa)	τ_s (MPa)	h_o (MPa)	h_s (MPa)	γ_o	γ_{oI}	$f_{\alpha\beta}$	$f_{\alpha\beta I}$	q	q_I
(110)[111]	13.7	16.4	292.262	1.4	0.25	0.25	10.0	9.9	0.0	0.0
(112)[111]	13.07	16.344	49.03325	39.2266	0.1	0.1	0.34	0.3	0.0	0.0

4. RESULTS AND DISCUSSION

As mentioned in the previous section, the crystal plasticity is included by modelling the niobium as single crystals using Bassani & Wu [2, 24] hardening law. The set of hardening parameters used is given in Table 1, while Alumina shanks, polycrystalline niobium sheet and Alumina single crystals are always modelled as elastic material.

Five different orientations of niobium single crystals have been used for the simulation (see Table 2). In what follows next, the results of the energy release rate, strain distribution around the stationary crack-tip along with the plastic slip (strain) near the stationary crack-tip have been discussed for different orientations.

Table 2. Orientations of niobium single crystals used for simulations

Symbol	Orientation relationship
Orientation I	Nb(100)[001] | Sp(11−20)[0001]
Orientation II	Nb(110)[001] | Sp(11−20)[0001]
Orientation III	Nb(111)[−1−1−2] | Sp(11−20)[0001]
Orientation IV	Nb(100)[−0.146 −0.94 0.3] | Sp(11−20)[0001]
Orientation V	Nb(100)[−0.23 −0.94 0.25] | Sp(11−20)[0001]

The energy release rates for five different orientations (mentioned above) have been plotted against the strain at the stationary crack-tip in Fig. 4. The results depict that the change in crystal orientation influences the energy release rates only after the plastic deformation has started. The start of the plastic deformation is the point where the resolved shear stress of any slip system exceeds the initial yield stress τ_o, which can be monitored during the simulation run. The highest energy release rate is found for orientation II, which is a multiple slip orientation with (1−12)[−111], (−211)[111] and (211)[−111] systems playing a major role in the total plastic slip and eventually in the plastic strain (see Fig. 5). Figure 5 shows the relative magnitudes of the slip activity, where the slip activity at a radius of 15 μm from the crack tip is plotted for each of the activated slip systems relative to the polar angle; 0° coincides with the prolongation of the crack and 180° coincides with the single crystal niobium crack flank.

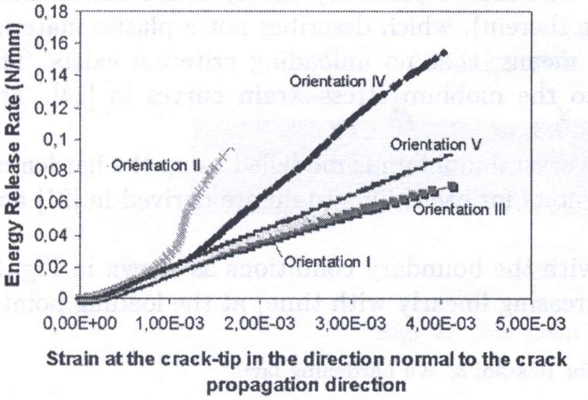

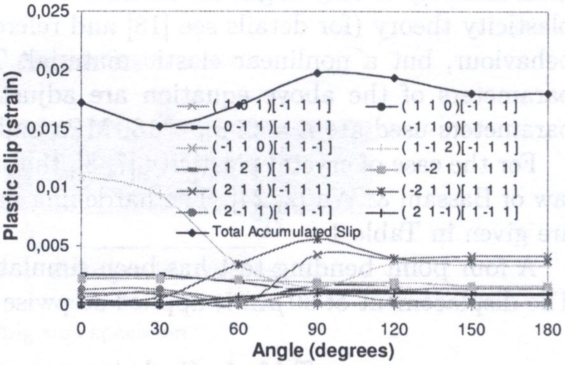

Fig. 4. Total energy release rate versus the strain at the crack tip for various orientation

Fig. 5. Plastic strain on slip systems at 15 μm radius from the tip of the stationary crack for orientation II

The contour plots of plastic slip (strain) on the above discussed three slip systems, as well as the total plastic slip (strain) for the orientation II along with the total logarithmic strain are plotted in Figs. 6(a–c), 11(b) and 12(b) to indicate the radial variation of the slip. The plastic region developed due to the plastic slip in (1−12)[−111] system is the largest one (Fig. 6(a)) and the plastic slip in this slip system dominates the total plastic slip (strain) region (Fig. 11(b)).

The orientations I and III were found to have the lowest energy release rates (see Fig. 4). For orientation I, the major contribution to the total slip comes from (112)[11−1], (121)[1−11], (1−21)[111], (12 1)[−111], (−211)[111] and (21−1)[1−11] slip systems (see Fig. 13). The contour plots of the slip on these systems along with the total accumulated slip and total logarithmic strain are plotted in Figs. 7(a–f), 11(a) and 12(a) to indicate the radial variation of the slip. The plastic region developed due to the plastic slip in (21−1)[1−11] system is the largest one (Fig. 7(f)) and the plastic slip in this slip system dominates the total plastic slip (strain) region (Fig. 11(a)).

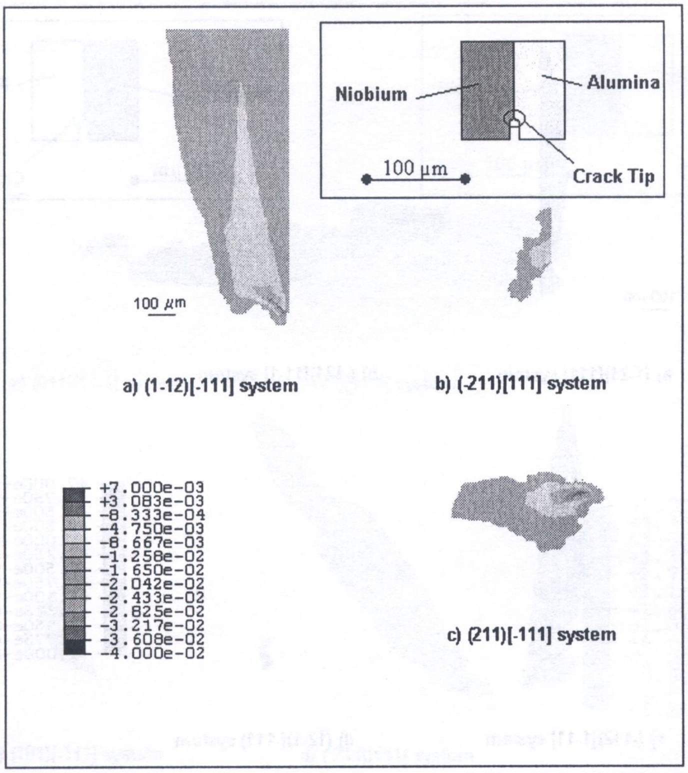

Fig. 6. Plastic strain on various slip systems at the tip of stationary crack for orientation II

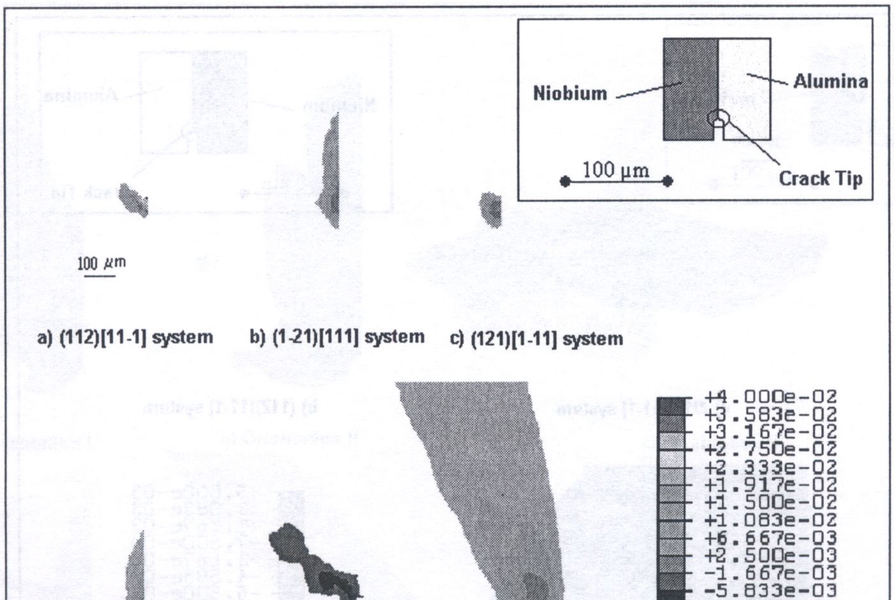

Fig. 7. Plastic strain on various slip systems at the tip of stationary crack for orientation I

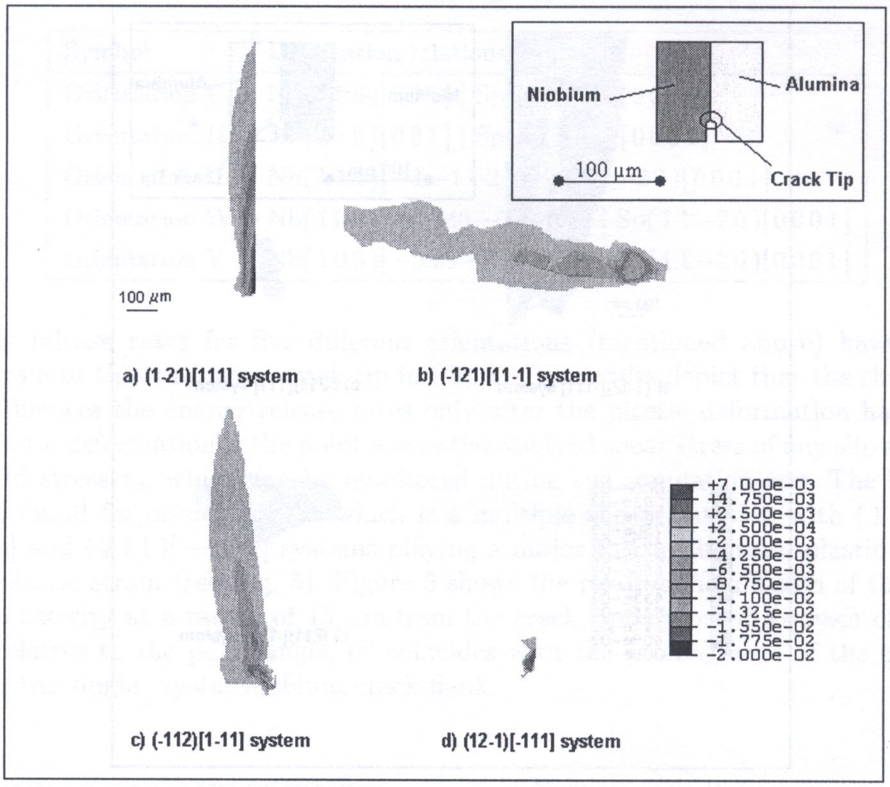

Fig. 8. Plastic strain on various slip systems at the tip of stationary crack for orientation III

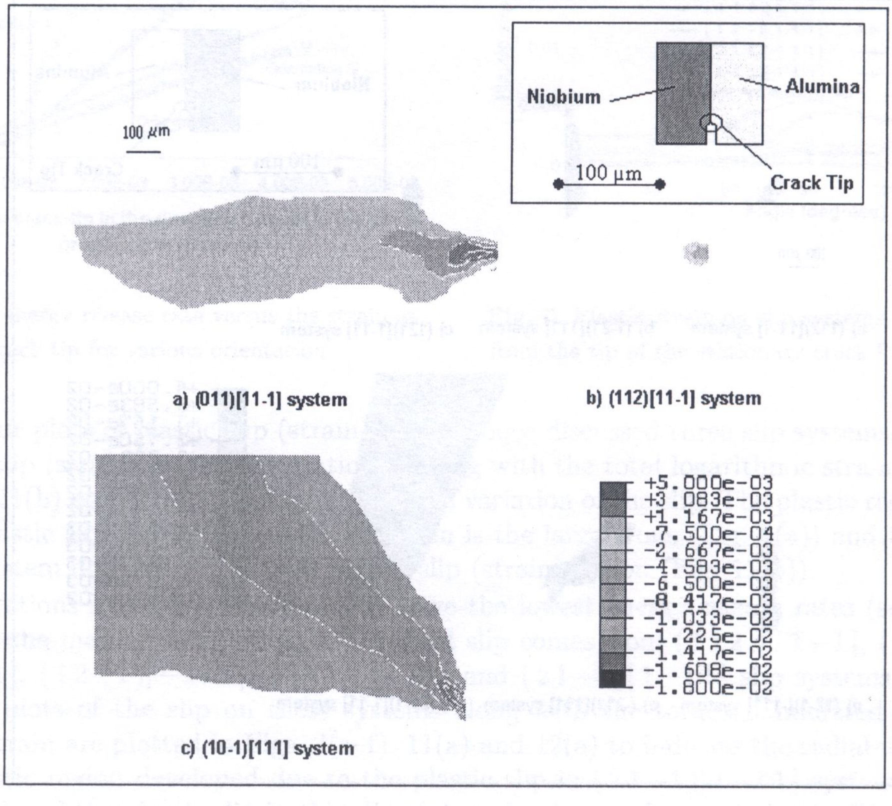

Fig. 9. Plastic strain on various slip systems at the tip of stationary crack for orientation IV

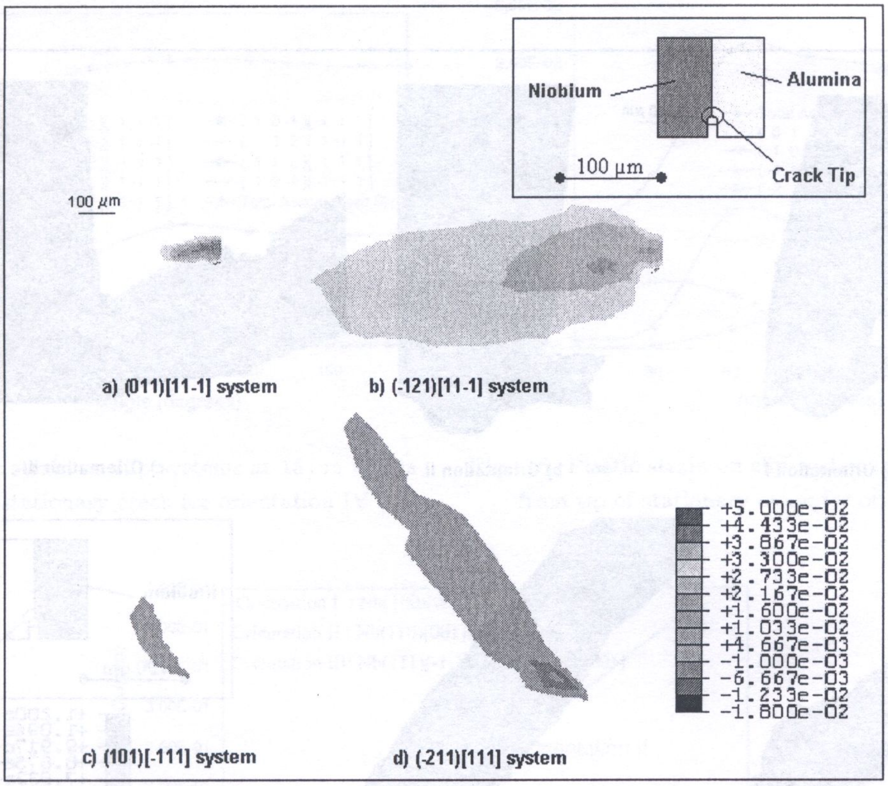

Fig. 10. Plastic strain on various slip systems at the tip of stationary crack for orientation V

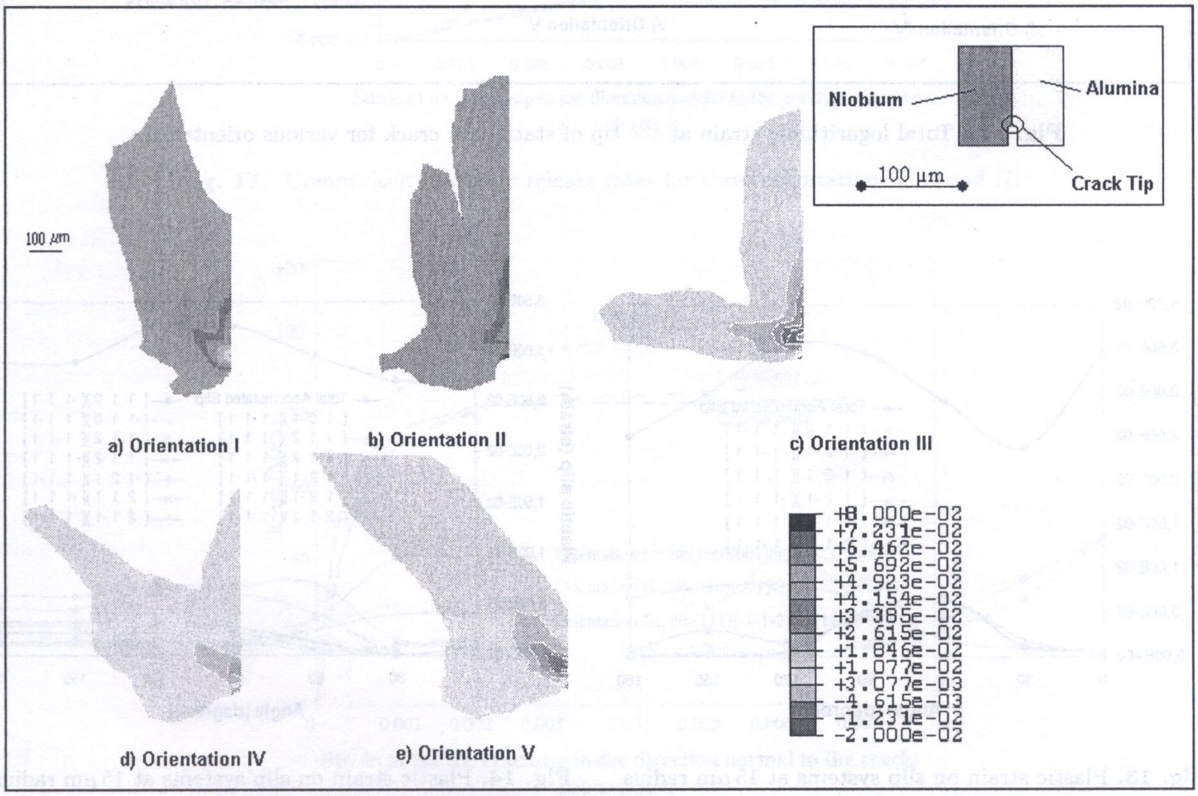

Fig. 11. Plastic cumulative slip (strain) on all slip systems at the tip of stationary crack for various orientations

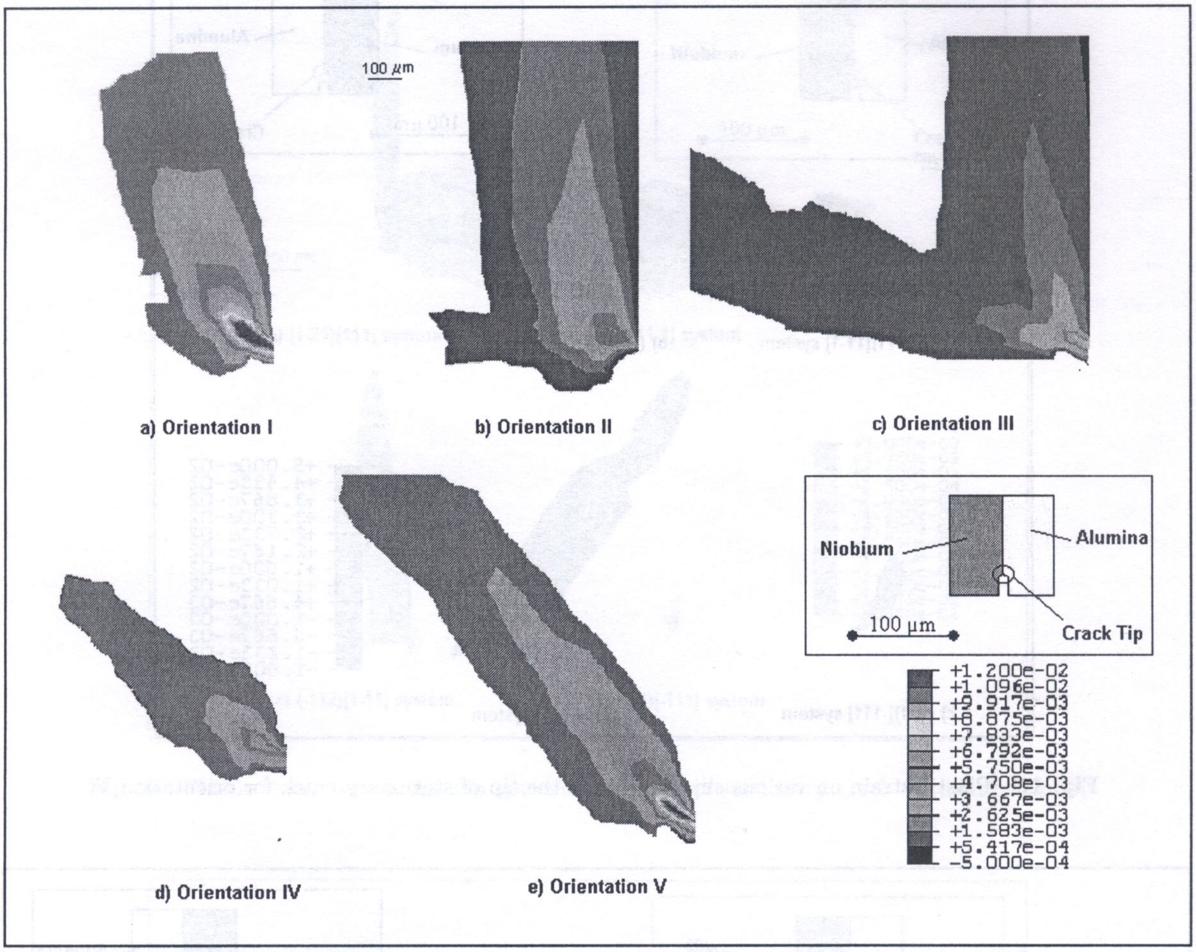

Fig. 12. Total logarithmic strain at the tip of stationary crack for various orientations

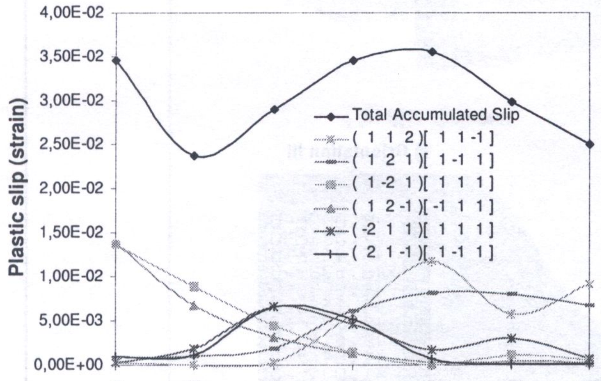

Fig. 13. Plastic strain on slip systems at 15 μm radius from tip of stationary crack for orientation I

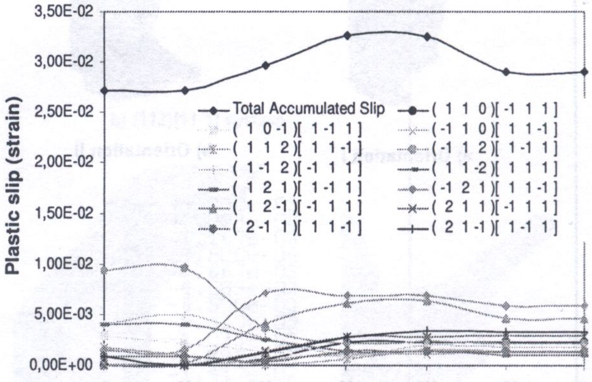

Fig. 14. Plastic strain on slip systems at 15 μm radius from tip of stationary crack for orientation III

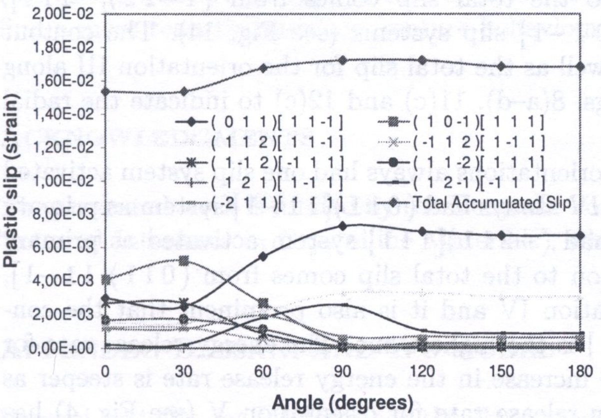

Fig. 15. Plastic strain on slip systems at 15 μm radius from tip of stationary crack for orientation IV

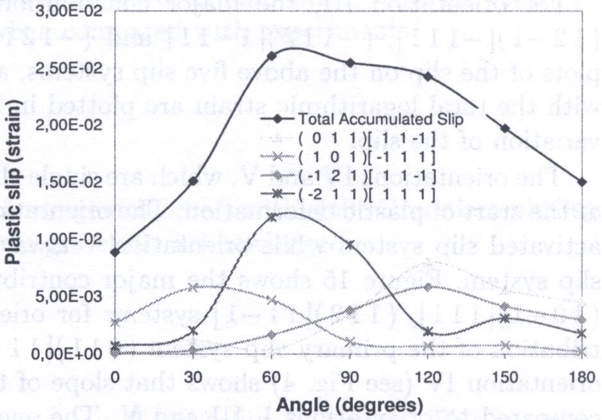

Fig. 16. Plastic strain on slip systems at 15 μm radius from tip of stationary crack for orientation V

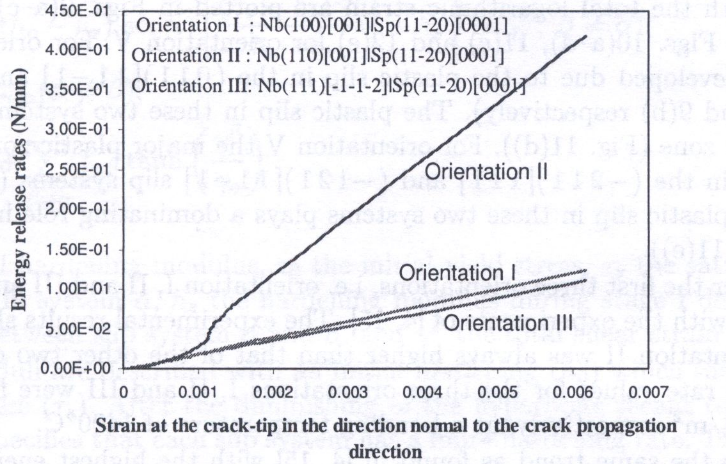

Fig. 17. Comparison of energy release rates for three orientations I, II and III

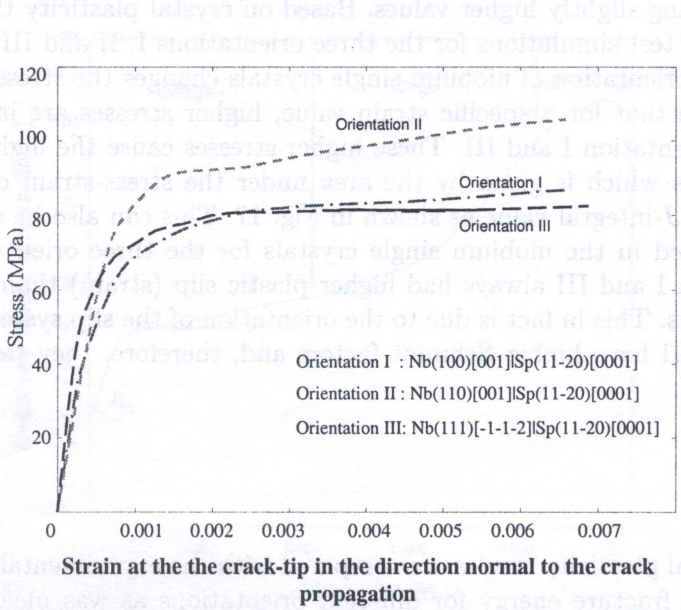

Fig. 18. Stress-strain curves for orientations I, II and III of uniaxial simulation

For orientation III, the major contribution to the total slip comes from (1−12)[−111], (12−1)[−111], (−112)[1−11] and (−121)[11−1] slip systems (see Fig. 14). The contour plots of the slip on the above five slip systems, as well as the total slip for the orientation III along with the total logarithmic strain are plotted in Figs. 8(a–d), 11(c) and 12(c) to indicate the radial variation of the slip.

The orientations IV and V, which are single slip orientations always had one slip system activated at the start of plastic deformation. The orientation IV always had (011)[11−1] system as primary activated slip system while orientation V always had (−211)[111] system activated as primary slip system. Figure 15 shows the major contribution to the total slip comes from (011)[11−1], (10−1)[111], (112)[11−1] systems for orientation IV and it is also prominent that the contribution of the primary slip system (011)[11−1] is the highest one. The energy release rate for orientation IV (see Fig. 4) shows that slope of the increase in the energy release rate is steeper as compared to orientations I, III and V. The energy release rate for orientation V (see Fig. 4) has almost the same trend as other orientations I and III. Figure 16 shows that the major contribution to the total slip comes from (011)[11−1], (101)[−111], (−121)[11−1] and (−211)[111] systems for orientation V and the contribution of the primary slip system (−211)[111] is the highest one. The contour plots of the slip on the different activated slip systems, as well as the total slip along with the total logarithmic strain are plotted in Figs. 9(a–c), 11(d) and 12(d) for orientation IV and Figs. 10(a–d), 11(e) and 12(e) for orientation V. For orientation IV the major plastic zones are developed due to the plastic slip in the (011)[11−1] and (10−1)[111] systems (Figs. 9(a) and 9(b) respectively). The plastic slip in these two systems dominates the total plastic slip (strain) zone (Fig. 11(d)). For orientation V the major plastic zones are developed due to the plastic slip in the (−211)[111] and (−121)[11−1] slip systems (Figs. 10(c) and 10(d) respectively). The plastic slip in these two systems plays a dominating role in the total plastic slip (strain) zone (Fig. 11(e)).

Now, we consider the first three orientations, i.e. orientation I, II and III and compare the energy release rate trends with the experiments of [4, 15]. The experimental results showed that the energy release rate of orientation II was always higher than that of the other two orientations I and III. The energy release rate values for the three orientations I, II and III were found to be 115 J/m^2, 370 J/m^2 and 112 J/m^2 respectively, at a bonding temperature of 1400°C.

Figure 17 shows the same trend as found in [4, 15] with the highest energy release rate found for orientation II while orientation I and III were almost having the same energy release rate values with orientation I having slightly higher values. Based on crystal plasticity the stress-strain curves of the uniaxial tension test simulations for the three orientations I, II and III are plotted in Fig. 18 which shows that the orientation of niobium single crystals changes the stress-strain behaviour and one can eventually see that for a specific strain value, higher stresses are induced for the case of orientation II than orientation I and III. These higher stresses cause the higher total energy of the niobium single crystals which is given by the area under the stress-strain curve. This ultimately ends up with a higher J-integral value as shown in Fig. 17. This can also be explained on the basis of the total slip induced in the niobium single crystals for the three orientations: Figs. 5, 13, 14 depict that orientation I and III always had higher plastic slip (strain) than orientation II for the same loading conditions. This in fact is due to the orientation of the slip systems as the slip systems for orientation I and III have higher Schmidt factors and, therefore, they tend to slip more easily than the orientation II.

5. CONCLUSION

In this work, the crystal plasticity results are compared with the experimental results and show that there is a variation in fracture energy for different orientations as was measured in experiments. Based on the contribution of the plastic slip (strain) of activated slip systems for various orientations the difference in the energy release rate was explained As the interface strength plays an important role in the fracture energy, therefore, different cohesive laws will be implemented in the future to find a more realistic interface fracture behaviour, when compared with experiments.

ACKNOWLEDGMENTS

The presented work is funded by the Deutsche Forschungsgemeinschaft within the Graduiertenkolleg "Internal Interfaces in Crystalline Materials", which is gratefully acknowledged.

APPENDIX: BASSANI AND WU MODEL

Bassani and Wu model describes the three stage hardening of crystalline materials. This model is based upon the analytical characterization of the hardening moduli at any stage during deformation (Fig. 19). Their expression for self and latent hardening depends on the shear strain γ^{α} of all slip systems,

$$\begin{aligned} h_{\alpha\alpha} &= \left\{ (h_o - h_s) \sec h^2 \left[\frac{(h_o - h_s)\gamma^{\alpha}}{\tau_s - \tau_o} \right] + h_s \right\} G(\gamma^{\beta};\ \beta \neq \alpha), \\ h_{\alpha\beta} &= q h_{\alpha\alpha} (\alpha \neq \beta), \\ G(\gamma^{\beta};\ \beta \neq \alpha) &= 1 + \sum_{\beta \neq \alpha} f_{\alpha\beta} \tanh \left(\frac{\gamma^{\beta}}{\gamma_o} \right), \end{aligned}$$

where, h_0 is the initial hardening modulus, τ_0 the initial yield stress, τ_s the saturation stress, $\gamma^{(\alpha)}$ the total shear strain in system α, h_s the hardening modulus during stage I deformation, $f_{\alpha\beta}$ the interaction strength between slip system α and β, and γ^{β} the total shear strain in slip system β.

The hardening moduli are described with an initial hardening (h_0) which saturates after reaching resolved shear stress (τ_s). After the diminishing of the hyperbolic secant term, the saturation hardening (h_s) term specifies that each slip system has a finite hardening rate. The function G deals implicitly with cross-hardening that occurs between slip systems during stage II.

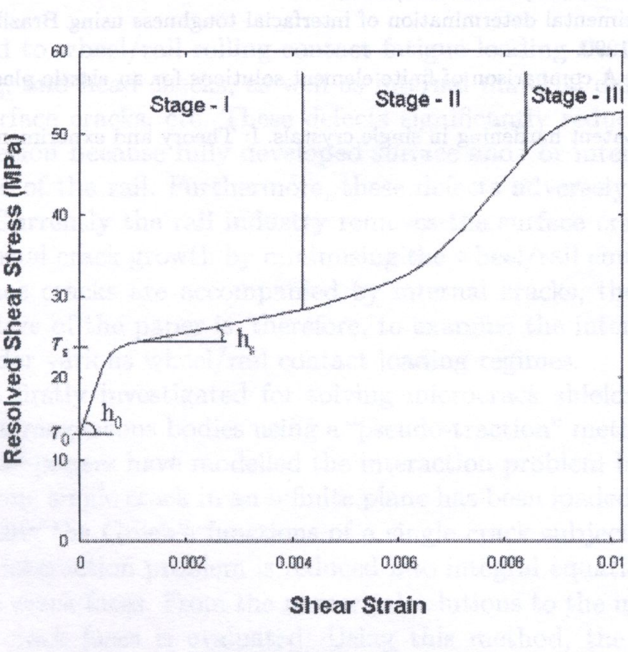

Fig. 19. Bassani & Wu Model

REFERENCES

[1] ABAQUS Version 6.4, Hibbitt, Karlsson, Sorensen.

[2] J.L. Bassani, T.-Y. Wu. Latent hardening in single crystals. II: Analytical characterization and predictions. *Philos. Trans. Roy. Soc. London A*, **435**: 21–41, 1991.

[3] W. Brocks, I. Scheider. *Numerical Aspects of the Path-Dependence of the J-Integral in Incremental Plasticity.* Technical Note GKSS/WMS/01/08, internal report, 2001.

[4] R.M. Cannon, D. Korn, G. Elssner, M. Rühle. Fracture properties of interfacially doped Nb-Al_2O_3 bicrystals. II: Relation of interfacial bonding, chemistry and local plasticity. *Acta Materialia*, **50**: 3903–3925, 2002.

[5] C.P. Cherepanov. Crack propagation in continuous media. *Appl. Math. Mech.*, **31**: 476–488, 1967.

[6] L.B. Freund. *Dynamic Fracture Mechanics*. Cambridge University Press, 1998.

[7] R. Hill, J.R. Rice. Constitutive analysis of elastic-plastic crystals at arbitrary strain. *J. Mech. Phys. Solids*, **20**: 401–413, 1972.

[8] Y. Huang. *A User Material Subroutine Incorporating Single Crystal Plasticity in the ABAQUS Finite Element Program.* Mech. Report 178, Division of Applied Sciences, Harvard University, Cambridge, MA, 1991.

[9] J.W. Hutchinson, Z. Suo. Mixed mode cracking in layered materials. *Advances Appl. Mech.*, **29**: 63–191, 1992.

[10] C.G. Hwang, P.A. Wawrzynek, A.K. Tayebi, A.R. Ingraffea. On virtual crack extension method for calculation of the rates of energy release rate. *Engrg. Fracture Mech.*, **59**: 521, 1998.

[11] C. Kohnle, O. Mintchev, D. Brunner, S. Schmauder. Fracture of metal–ceramic interfaces. *Comput. Mater. Sci.*, **19**: 261, 2000.

[12] C. Kohnle, O. Mintchev, D. Brunner, S. Schmauder. Fracture of metal–ceramic interfaces. In: *Proc. Material Week*, 2000.

[13] available from www.goodfellow.com.

[14] C. Kohnle, O. Mintchev, D. Brunner, S. Schmauder. Elastic and plastic fracture energies of metal–ceramic joints. *Comput. Mater. Sci.*, **25**: 272, 2002.

[15] D. Korn, G. Elssner, R.M. Cannon, M. Rühle. Fracture properties of interfacially doped Nb-Al_2O_3bicrystals. I: Fracture characterisitics. *Acta Materialia*, **50**: 3881–3901, 2002.

[16] R. Krueger. The virtual crack closure technique: History, approach and applications. ICASE Report no. 2002-10.

[17] L.H. Larsson. A calculational round robin in elastic-plastic fracture mechanics. *Int. J. Press. Vess. Piping*, **11**: 207, 1983.

[18] O. Mintchev, J. Rohde, S. Schmauder. Mesomechanical simulation of crack propagation through graded ductile zones in hardmetals. *Comput. Mater. Sci.*, **13**: 81, 1998.

[19] W. Ramberg, W.R. Osgood. *Description of Stress–Strain Curves by Three Parameters.* NASA Technical Note No 902, 1945.

[20] J.R. Rice. A path independent integral and the approximate analysis of strain concentrations by notches and cracks. *J. Appl. Mech.*, **35**: 379–386, 1968.

[21] A. Siddiq, S. Schmauder. Simulation of deformation behaviour of niobium single crystals using crystal plasticity. *Steel Grips: J. Steel Rel. Materials*, **3**: 281–286, 2005.

[22] J.S. Wang, Z. Suo. Experimental determination of interfacial toughness using Brazil-nut-sandwich. *Acta Metallurgica*, **38**: 1279–1290, 1990.

[23] W.K. Wilson, J.R. Osias. A comparison of finite element solutions for an elastic-plastic crack problem. *Int. J. Fracture*, **14**: R95, 1978.

[24] T.-Y. Wu, J.L. Bassani. Latent hardening in single crystals. I: Theory and experiments. *Math. Phys. Sci.*, **435**: 21-41, 1993.